The charge density induced by a point test charge in a magnetized electron gas

1995 J. Phys.: Condens. Matter 7 6545

(http://iopscience.iop.org/0953-8984/7/32/020)

J. Phys.: Condens. Matter 7 (1995) 6545–6560. Printed in the UK

The charge density induced by a point test charge in a magnetized electron gas

F Perrot and A Grimaldi

Commissariat à l'Energie Atomique, Centre d'Etudes de Limeil-Valenton, 94195 Villeneuve St Georges Cédex, France

Received 11 April 1995

Abstract. The charge density induced by a point charge immersed in an electron gas, in the presence of a magnetic field, is studied using linear response theory, for a range of metallic densities and fields up to 4×10^5 T. The response function, inclusive of an approximate field factor for exchange and correlation effects, is first presented in the current density functional theory formalism. Numerical methods are then described. Results for the embedding energy of the point charge and non-spherical deformation of the charge density are reported. They are discussed in the perspective of building a statistical model of electronic structure in the presence of strong magnetic fields.

1. Introduction

The fast development of high-magnetic-field research with generators producing fields up to $B = 1000$ T [1] prompts studies of the electronic structure of materials submitted to intense fields. For instance, the change in resistivity and equation of state of metals under these extreme conditions is of primary interest for predicting and explaining the experiments. Such studies of the electronic structure of magnetic systems were initiated twenty years ago, using Thomas–Fermi-like models, for applications in the domain of astrophysics [2–12]. As is known from their intensive application to the case $B = 0$, the approaches based on statistical theories are particularly well suited for equation of state calculations. Their extension to the magnetic case raises a number of difficulties. Because the interesting quantity is the *change* in some property with the magnetic field, the theory must be able to treat continuously increasing magnetic field intensities, starting from $B = 0$. In this respect, models restricted to conditions where the first Landau band only is populated are of limited interest. It follows from this remark that, since low fields are equivalent to large wave vectors in the magnetic response function, the low-q corrections involved in a first-order gradient expansion are not sufficient. A second difficulty is related to the geometry. Whereas the solution of the statistical equations for a compressed atom is spherically symmetric in the $B = 0$ case, the charge density undergoes a non-spherical deformation when a strong magnetic field is applied. This non-spherical effect does not appear at the Thomas–Fermi level of approximation, but results from non-local contributions in the kinetic energy functional [8]. These remarks imply that the range of wave vectors which must be accurately treated has to be chosen with care when one attempts to define a relevant statistical approximation.

The present work is a preliminary study whose aim is to determine the domain of densities and magnetic fields where the intermediate wave vectors q (typically $0.1 \leqslant ql \leqslant$

0953-8984/95/326545+16$19.50

10, with l the magnetic length) play an important role in the description of the charge density. This importance is directly related to the *magnitude of the non-spherical effects*. Thus, it is useful to know, for a given average electron density, above what field intensity the non-spherical deformation begins to be significant and must be included in the models, as a first-order perturbation or to all orders. This is our main object in this work. A simplified problem is solved which, although it does not represent any true real system, particularly at low average electron density, is thought to describe correctly the trends of the non-spherical deformation. We consider a coulombic test charge immersed in a uniform electron gas and calculate the electron charge distribution induced around it, using the *magnetic linear response* function. The analysis of the displaced electron charge in Legendre polynomials at several distances from the test charge shows the importance of the non-spherical components. Another quantity of interest, relevant to equation of state studies, the *embedding energy* of the test charge, is calculated.

The paper is organized as follows. Section 2 is devoted to a presentation of magnetic linear response in the framework of current density functional theory, with a particular emphasis on the *local field corrections*. In section 3, we describe the density profile calculations and comment on some numerical aspects. The results are presented and discussed in section 4.

2. Linear response function in a magnetic field

2.1. Connection with energy functionals

The current density functional theory (CDFT) provides a very convenient framework for the discussion of the linear response function of an electron gas in a magnetic field [13]. Let us start with the CDFT expression of the total energy:

$$E[n(r), j_p(r)] = T_s[n(r), j_p(r)] + E_H[n(r)] + \int n(r)\left[V_{ext}(r) + \frac{e^2}{2m}A^2(r)\right] d^3r$$
$$+e\int j_p(r)\cdot A(r)\, d^3r + E_{xc}[n(r), j_p(r)]. \tag{1}$$

In this expression, e is the electron charge, m the electron mass, T_s is the non-interacting 'pseudo'-kinetic energy (corresponding to the operator $-\hbar^2/2m\nabla^2$), E_H is the Hartree energy and E_{xc} is the exchange and correction (xc) energy. The electron density is $n(r)$ and $j_p(r)$ is the paramagnetic (orbital) current. The external potential has a scalar component V_{ext} and a vector component A such that the applied magnetic field is $B = \mathrm{curl}\, A$. In this study, we neglect the magnetic moment Landé g factor. The total physical current J is given by

$$J(r) = j_p(r) + (e/m)n(r)A(r). \tag{2}$$

The CDFT has demonstrated that the total energy in (1) is a unique functional of both $n(r)$ and $j_p(r)$ which reaches its minimum for the exact values of these independent quantities. In practice, it is more convenient to work with a new variable

$$u(r) = j_p(r)/n(r) \tag{3}$$

instead of $j_p(r)$. The Kohn–Sham equations associated with the CDFT are

$$\delta T_s[n(r), u(r)]/\delta n(r) + \delta E_{xc}[n(r), u(r)]/\delta n(r) + V_{ext}(r) + V_H(r)$$
$$+eu(r)\cdot A(r) + (e^2/2m)A^2(r) = \mu \tag{4}$$

$$\delta T_s[n(r), u(r)]/\delta u(r) + \delta E_{ex}[n(r), u(r)]/\delta u(r) + en(r)A(r) = 0. \tag{5}$$

Now we consider the case of the uniform system of density n with $V_{ext} = 0$. In this case, the physical current J vanishes, so the paramagnetic current is $j_{p0}(r) = -(e/m)nA(r)$. Then, a small scalar perturbing potential δV (including the external and Hartree screening potentials) is applied, and we study the linear response δn and δu. Linearizing (4) and (5) gives

$$(S_s + S_{xc})\delta n + (U_s + U_{xc}) \cdot \delta u + \delta V = 0 \tag{6}$$

$$(U_s + U_{xc})^\dagger \delta n + (\mathbf{M}_s + \mathbf{M}_{xc})\delta u = 0 \tag{7}$$

where the following notations are used:

$$\begin{aligned} S_s &= \{\delta^2 T_s[n(r), u(r)]/\delta n(r)\delta n(r)\}|_0 \\ S_{xc} &= \{\delta^2 E_{xc}[n(r), u(r)]/\delta n(r)\delta n(r)\}|_0 \end{aligned} \tag{8}$$

$$\begin{aligned} U_s &= \{\delta^2 T_s[n(r), u(r)]/\delta n(r)\delta u(r)\}|_0 + eA(r) \\ U_{xc} &= \{\delta^2 E_{xc}[n(r), u(r)]/\delta n(r)\delta u(r)\}|_0 \end{aligned} \tag{9}$$

$$\begin{aligned} \mathbf{M}_s &= \{\delta^2 T_s[n(r), u(r)]/\delta u(r)\delta u(r)\}|_0 \\ \mathbf{M}_{xc} &= \{\delta^2 E_{xc}[n(r), u(r)]/\delta u(r)\delta u(r)\}|_0. \end{aligned} \tag{10}$$

The functional derivatives in (8) are scalar quantities, those in (9) are vectors and those in (10) are tensors. The notation $|_0$ means that these derivatives are taken for the reference (uniform) system. From (6) and (7), we obtain for the interacting response function χ

$$1/\chi = \delta V/\delta n = -(S_s + S_{xc}) - (U_s + U_{xc})^\dagger \cdot (\mathbf{M}_s + \mathbf{M}_{xc})^{-1}(U_s + U_{xc}). \tag{11}$$

The counterpart of this function if xc effects are omitted is

$$1/\chi^0 = -S_s - U_s^\dagger \cdot \mathbf{M}_s^{-1} U_s. \tag{12}$$

A lot of work has been done on this response function, and explicit expressions for χ^0 may be found in the literature [14–17].

2.2. *Local field corrections*

The local field factor X due to xc effects is defined by writing down the equation relating δn and δV:

$$(1/\chi^0)\delta n = \delta V + X\delta n \tag{13a}$$

$$= (1/\chi)\delta n + X\delta n \tag{13b}$$

so

$$X = S_{xc} + (U_s + U_{xc})^\dagger \cdot (\mathbf{M}_s + \mathbf{M}_{xc})^{-1}(U_s + U_{xc}) - U_s^\dagger \cdot \mathbf{M}_s^{-1} U_s. \tag{13c}$$

In the absence of a magnetic field, the local field factor reduces to S_{xc}. The magnetic field modifies X in two ways. First, S_{xc} itself is different in the presence of B; second, there are additional terms in (13c). A common approach is to estimate X in the local density approximation (LDA). In the LDA, the unknown exact functional $E_{xc}[n(r), u(r)]$ is approximated using local values of the xc energy of the uniform electron gas $E_{xc}^u(n, \omega)$. At each point in space, n is replaced with $n(r)$ and the cyclotron frequency ω with $\omega(r) = |\nabla \times u(r)|$ (in the uniform electron gas, $\omega = |\nabla \times u_0(r)|$ as a consequence of $J(r) = 0$):

$$E_{xc}[n(r), u(r)] \to E_{xc}^u(n(r), \omega(r)) = \int f_{xc}(n(r), \omega(r))\, \mathrm{d}^3 r. \tag{14}$$

Thus, an approximate S_{xc} can be calculated from (8) using the fit proposed by Skudlarski and Vignale for $E^u_{xc}(n,\omega)$ that they computed in the RPA approximation [18].

A first approximation for the additional term in X is to evaluate it entirely in the LDA, that is using the kinetic functional of the uniform system:

$$T_s[n(r),u(r)] = \int f_s(n(r),\omega(r))\,d^3r + \int \frac{m}{2} n(r)u^2(r)\,d^3r \tag{15}$$

to calculate the quantities entering (13*c*). This LDA approximation provides the exact low-q limit of the functional T_s. We easily obtain the following expressions in Fourier space:

$$S_s(q) = (f_s)''_{nn} + O(q^2)$$
$$U_s(q) = (f_s)''_{n\omega} e_z \times iq + O(q^2)$$
$$\mathbf{M}_s(q) = -mn\mathbf{I} + O(q^2) \qquad \mathbf{M}_{xc}(q) = O(q^2)$$

where $(f_s)''_{n\omega}$ is the second derivative of $f_s(n,\omega)$ with respect to the variables n and ω, e_z a unit vector in the direction of B, $\mathbf{I}$ the identity matrix and n the density of the uniform electron gas. With similar definitions for the xc contribution, we arrive at the following form of (13*c*), in the low-q limit:

$$X - S_{xc} = q_\perp^2 Y_{xc} + O(q^4) \tag{16a}$$
$$Y_{xc} = (1/mn)(|(f_s)''_{n\omega} + (f_{xc})''_{n\omega}|^2 - |(f_s)''_{n\omega}|^2) \tag{16b}$$

with $q_\perp$ the component of q perpendicular to the field. The right-hand side term of (16*a*), which vanishes identically when $B = 0$, is of order q^2. If this term were taken into account, the expansion of $S_{xc}(q)$ should be carried out to order q^2 also. For $B = 0$, the q^2 term in $S_{xc}(q)$ does not vanish entirely so that the approximation does not reduce to the standard LDA. Thus, to keep on with the same level of approximation as in the $B = 0$ case, these q^2 terms should be discarded, leading to the local field factor

$$X = S_{xc}(q=0) = (f_{xc}(n,\omega))''_{nn}.$$

Unfortunately, this approximation fails for large B because it produces roots in the static dielectric constant. Thus, the q dependence of X must be taken into account for large magnetic fields. Paralleling the approximation made in the $B = 0$ case [19], we write

$$X(q) = S_{xc}/(1 + q^2|S_{xc}|/2\pi) + q_\perp^2 Y_{xc}/(1 + q_\perp^2 l^2)^2. \tag{17}$$

The second term is roughly proportional to $|U_s \cdot U_{xc}|$. According to the results of Vignale and Skudlarski [20] relative to the current $J(q)$ beyond the LDA, $U_s(q)$ decreases rather fast with $q_\perp l$. To take this effect into account, we have divided the LDA form of $U_s(q)$ by $(1 + q_\perp^2 l^2)$, where l is the magnetic length such that

$$l^2 = \hbar/m\omega.$$

The same damping factor has been applied to $U_{xc}(q)$. With the form in (17) for $X(q)$ the dielectric constant

$$\varepsilon(q) = 1 - (4\pi e^2/q^2 + X(q))\chi^0(q)$$

has no zero anymore. But, clearly, a more fundamental study of the xc effects in the magnetic dielectric constant is called for.

2.3. *Explicit expression of the non-interacting response function*

The first complete analysis of the RPA response function of the electron gas in a magnetic field was performed by Greene and co-workers [14]. Many other studies of this function

have been reported more recently in the literature [15–17]. Here we reproduce the most compact form of $\chi^0(q)$ adapted to numerical calculations:

$$\chi^0(q) = -\frac{1}{\pi^2 l^3 \hbar\omega} \sum_{j=0}^{N} \sum_{i=0}^{\infty} K_{ij}(q_\perp l) \frac{1}{q_z l} \ln \left| \frac{(q_z l + k_j)^2 - k_i^2}{(q_z l - k_j)^2 - k_i^2} \right|. \tag{18}$$

The summation over spin results in a factor of two included in (18). This expression involves a double sum on Landau band indices j and i; j runs over the occupied bands and i over all the bands. In the logarithm, the momenta are defined as

$$k_j^2 = (2m/\hbar^2)(\mu - (j + \tfrac{1}{2})\hbar\omega)\, l^2 = 2(\mu/\hbar\omega - (j + \tfrac{1}{2})) \tag{19}$$

and similarly for k_i^2. Note that the latter is a negative quantity for $i > N$. The function K_{ij} is defined for $i \geqslant j$ by

$$K_{ij}(s) = (j!/i!)(s^2/2)^{i-j}[L_j^{i-j}(s^2/2)]^2 \exp(-s^2/2) \tag{20}$$

where L_j^{i-j} is a generalized Laguerre polynomial. If $i < j$ in the double sum, then the indices must be interchanged in K_{ij}.

It is clear from (18) that $\chi^0(q)$ is only a function of the reduced variable ql (the product of the wave vector with the magnetic length). Thus, the limit at large q is also the limit at large magnetic length, i.e. at small B. This means that the asymptotic form of $\chi^0(q)$ is that of the Lindhard function $\chi^L(q)$. We have checked this conclusion numerically. In fact, the convergence of the sum on i in (18) is very slow. In figures 1 and 2 we see examples of how the magnetic response function reduces to the Lindhard function at large values of $s = q_\perp l$. If M is the maximum value of i that has to be included in the sum to reach convergence, M increases very fast with the value of s for which continuity is observed. For a given M, the value of s for which the asymptotic form is reached is rather insensitive to $y = \mu/\hbar\omega$. Thus, the wave vector above which the two response functions become equivalent is of the form $q/k_F = \text{constant}/\sqrt{y}$, where k_F is the Fermi momentum.

3. Calculation of the density displaced by a test charge

3.1. Electron density

Starting from (13*a*) with the external potential δV_{ext} of a point charge, we obtain the density in Fourier space:

$$\delta n(q) = F(q) 4\pi e^2/q^2 \tag{21a}$$

$$F(q) = \chi^0(q)/[1 - (4\pi e^2/q^2 + X(q))\chi^0(q)]. \tag{21b}$$

Figures 3 and 4 show the behaviour of $F(q)$ (with $q_z = 0$) in two typical cases. In figure 3, for $r_s = 2$, $B = 0.2B_0$ ($B_0 = 2.35 \times 10^9$ G), there is a kink in the curve due to the existence of a peak in $\chi^0(q)$ because two Landau bands are populated. In the case of figure 4 ($r_s = 2$, $B = 2B_0$), the Fermi level lies in the first Landau band so this effect does not appear. In coordinate space, the charge density is

$$\delta n(r) = (2\pi)^{-2} l^{-3} \int_0^\infty s\, ds\, J_0\left(s\frac{\rho}{l}\right) \int_{-\infty}^{+\infty} dt \cos\left(t\frac{z}{l}\right) F(q) \frac{4\pi e^2}{q^2} \tag{22}$$

where J_0 is the Bessel function, l the magnetic length, ρ the component of r perpendicular to B and z the component along B; s is the component of ql perpendicular to B and t the component of ql along B.

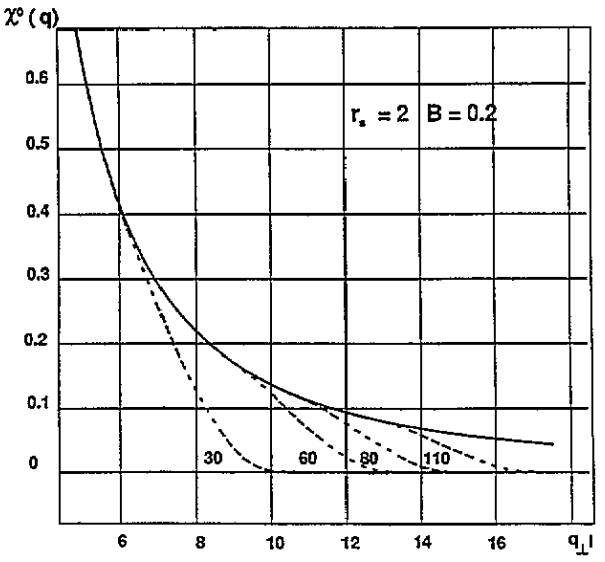

Figure 1. The response function $\chi^0(q)$ for the magnetized electron gas at $r_s = 2$ and $B/B_0 = 0.2$, as a function of $q_\perp l$, for $q_z l = 0$. Several curves are presented (dashed lines) corresponding to increasing maximum values M (30, 60, 80 and 110) of the band index in the sum over excited Landau bands (see (18)). Full convergence is obtained for $M \to \infty$. The solid curve is the Lindhard asymptotic form.

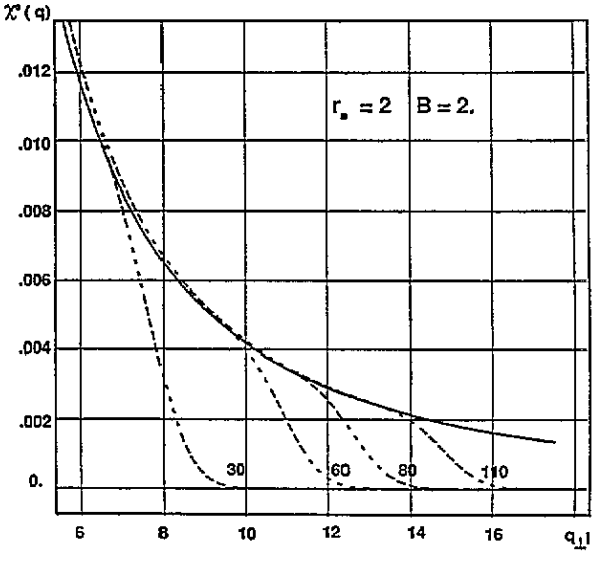

Figure 2. The same as figure 1, but for $B/B_0 = 2$.

For small values of the magnetic field, the treatment of large wave vectors is easier if the difference between $F(q)$ and its limit at zero field is introduced. This limit is obtained

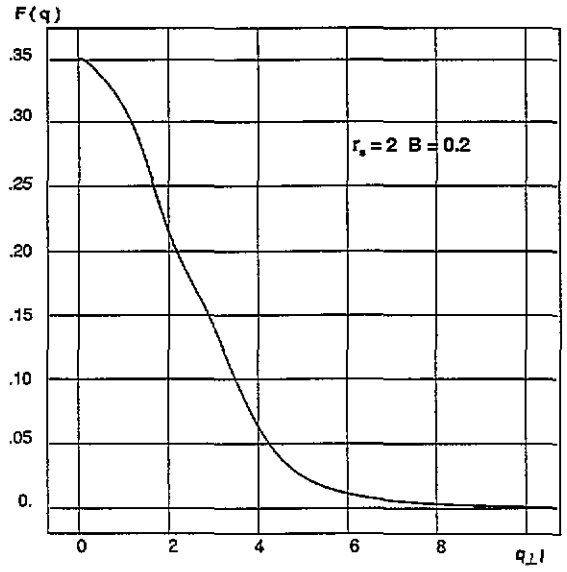

Figure 3. The full density response function $F(q)$, such that $\delta n(q) = F(q)\delta V_{ext}(q)$ for the magnetized electron gas at $r_s = 2$ and $B/B_0 = 0.2$, as a function of $q_\perp l$, for $q_z l = 0$.

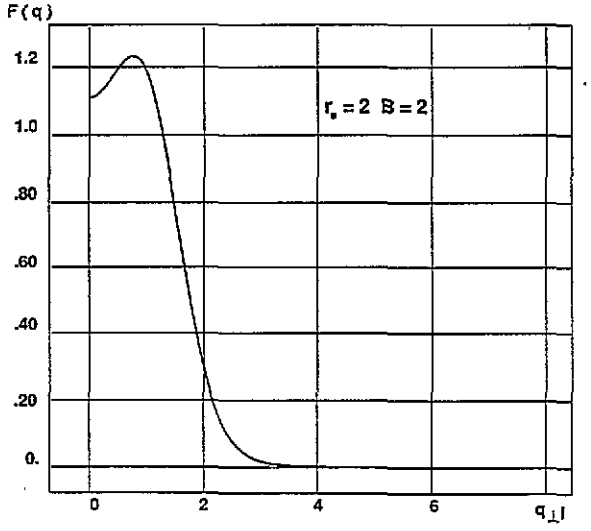

Figure 4. The same as figure 3, but for $B/B_0 = 2$.

by replacing $\chi^0(q)$ with the Lindhard form $\chi^L(q)$ in (21). Thus, the density becomes

$$\delta n(r) = (2\pi)^{-2} l^{-3} \int_0^\infty s\,\mathrm{d}s\, J_0\left(s\frac{\rho}{l}\right) \int_{-\infty}^{+\infty} \mathrm{d}t\, \cos\left(t\frac{z}{l}\right) (F(q) - F^L(q)) \left(\frac{4\pi e^2}{q^2}\right)$$
$$+2(2\pi)^{-2} l^{-3} \int_0^\infty u^2\,\mathrm{d}u\, j_0\left(u\frac{r}{l}\right) F^L(q) \left(\frac{4\pi e^2}{q^2}\right). \tag{23}$$

Table 1. Values of the second-order energy δE defined in (24), in Hartrees, and of the charge density $\delta n(0)$ on the test charge, in a_0^{-3} (23), for various values of the electron density parameter r_s and of the magnetic field. N is the index of the highest populated Landau band. For the energy and the charge density, two series of numbers are shown, one with no exchange and correlation contribution in the response function ($X = 0$) and the other with the local field factor $X(q)$ defined in (17).

			δE		$\delta n(0)$	
r_s	B/B_0	N	$(X=0)$	δE	$(X=0)$	$\delta n(0)$
1	0.0		−0.5863	−0.6077	0.3786	0.3907
	0.2	8	−0.5851	−0.6063	0.3781	0.3901
	0.5	3	−0.5927	−0.6147	0.3823	0.3947
	1.0	1	−0.5906	−0.6124	0.3811	0.3935
	2.0	0	−0.5872	−0.6102	0.3789	0.3919
2	0.0		−0.3749	−0.3963	0.08237	0.08630
	0.2	1	−0.3720	−0.3876	0.08207	0.08499
	0.5	0	−0.3754	−0.3982	0.08217	0.08631
	1.0	0	−0.4597	−0.5029	0.10370	0.11240
	2.0	0	−0.5342	−0.5944	0.15110	0.16990
3	0.0		−0.2853	−0.3060	0.03335	0.03530
	0.2	0	−0.2806	−0.2997	0.03287	0.03465
	0.5	0	−0.3464	−0.3855	0.04235	0.04658
	1.0	0	−0.3945	−0.4467	0.06055	0.06942
	2.0	0	−0.4332	−0.5028	0.09126	0.11040
4	0.0		−0.2339	−0.2538	0.01748	0.01864
	0.2	0	−0.2570	−0.2868	0.01911	0.02086
	0.5	0	−0.3077	−0.3509	0.02826	0.03236
	1.0	0	−0.3398	−0.3967	0.04210	0.05074
	2.0	0	−0.3663	−0.4388	0.06290	0.08016
5	0.0		−0.1998	−0.2190	0.01057	0.01134
	0.2	0	−0.2373	−0.2699	0.01329	0.01486
	0.5	0	−0.2747	−0.3206	0.02089	0.02486
	1.0	0	−0.2989	−0.3580	0.03119	0.03916
	2.0	0	−0.3200	−0.3920	0.04712	0.06173

The last contribution, where j_0 stands for the spherical Bessel function with $u = ql$, is calculated in spherical symmetry. The very large momenta, which are necessary for an accurate description of the density close to the test charge, are included with much less numerical effort, and the integration domain for the first contribution can be reduced.

3.2. Second-order energy

Using the CDFT formulation of section 2, it is easy to establish the expression of the test charge immersion energy in the magnetized electron gas. The first-order contribution (in δV_{ext}) is the chemical potential μ. The second-order contribution is

$$\delta E = \frac{1}{2}(2\pi)^{-3} \int \frac{4\pi e^2}{q^2} F(q) \frac{4\pi e^2}{q^2} \mathrm{d}^3 q. \tag{24}$$

The subtraction–addition technique described just above can also be used in the energy calculation when necessary.

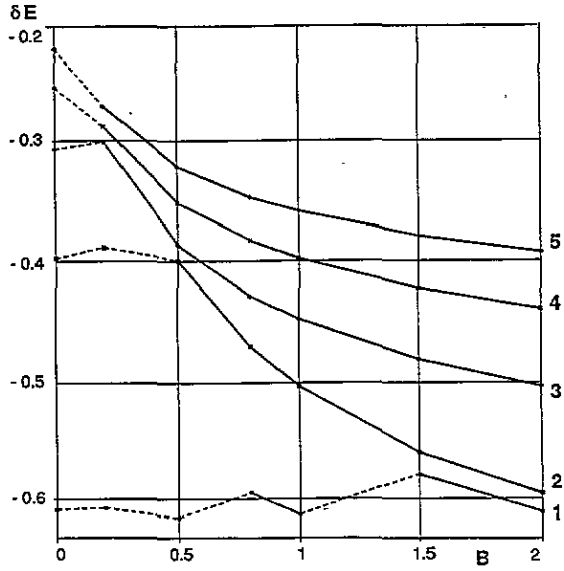

Figure 5. The second-order embedding energy of the point charge in the magnetized electron gas, in Hartree units, as a function of B/B_0 and for five values of r_s (1, 2, 3, 4 and 5). Solid curves join points having the same highest populated Landau band only.

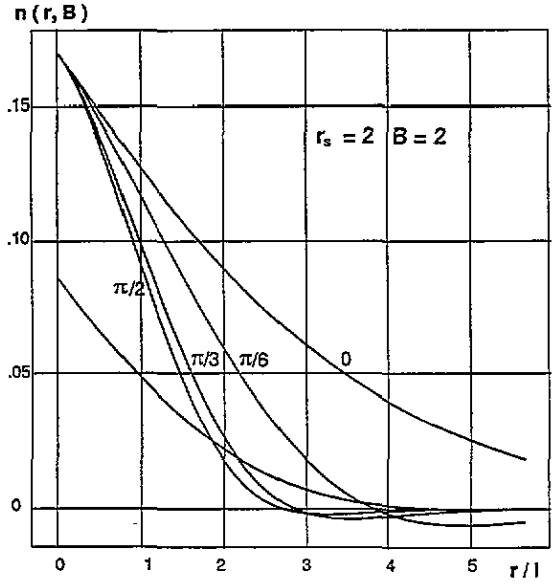

Figure 6. The charge density induced in the magnetized electron gas, as a function of distance in units of the magnetic length, at $r_s = 2$ and $B/B_0 = 2$. The four highest curves correspond to four directions with respect to $\mathcal{B}(\theta = 0)$. The lowest curve shows the density in the absence of a magnetic field.

3.3. The non-spherical shape of the density

We arrive here at the motivation of this study: the non-spherical deformation of the density induced by the magnetic field. The density $\delta n(r)$ calculated as described above is analysed

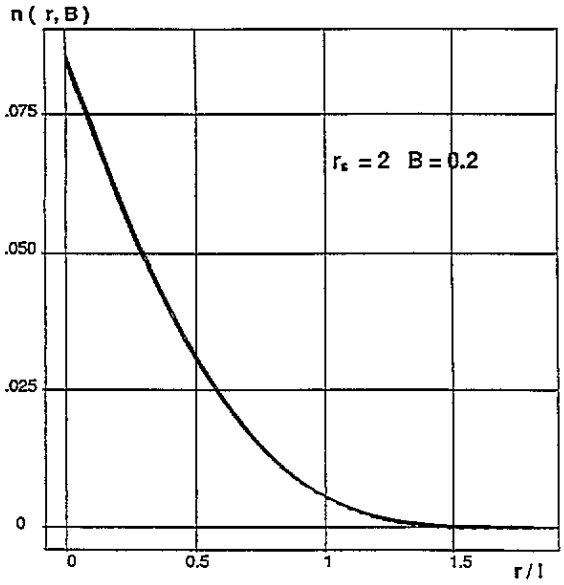

Figure 7. The same as figure 6, but for $B/B_0 = 0.2$.

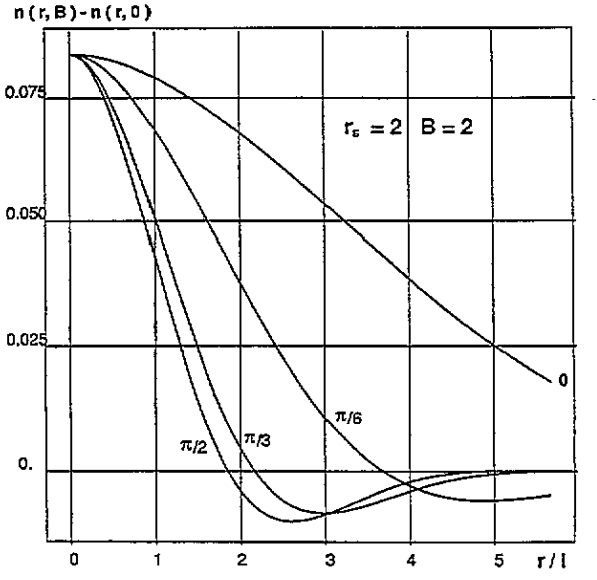

Figure 8. The difference between the charge densities with and without the magnetic field, at $r_s = 2$ and $B/B_0 = 2$, along four directions at angles $\theta = 0$, $\pi/6$, $\pi/3$ and $\pi/2$ with the field.

in Legendre polynomials. At a given distance from the test charge, one writes

$$\delta n(r) = \sum_{l=0}^{\infty} a_l(r) P_l(\cos\theta) \tag{25}$$

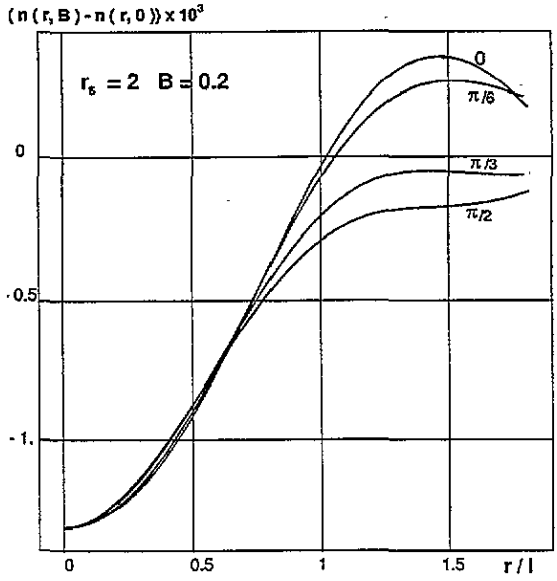

Figure 9. The same as figure 8, but for $B/B_0 = 0.2$.

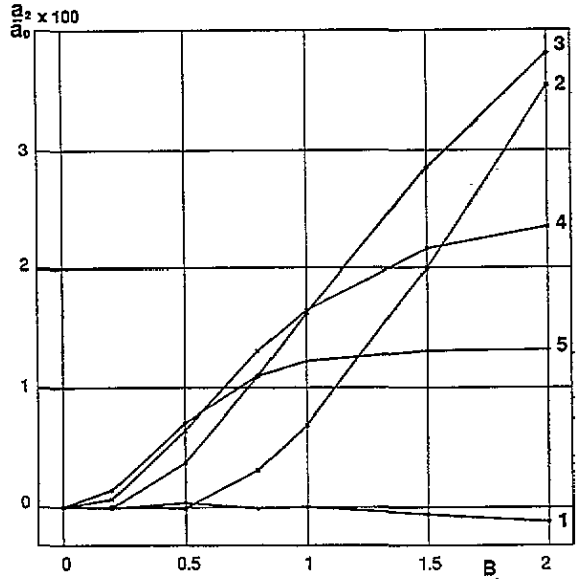

Figure 10. The ratio of the coefficient a_2 of the first non-spherical Legendre polynomial in the expansion of the charge density to the spherical component coefficient a_0 (see (25)), versus magnetic field B/B_0 and for the five values of r_s. The distance at which the expansion is done is $r = r_s/2$.

where θ is the angle between r and the magnetic field. This expansion involves even angular momenta only. The ratio of the coefficients a_1 to a_0 gives a measure of the non-spherical shape of the density.

Table 2. The non-sphericity of the charge density displaced around a test charge in a magnetized electron gas. The electron gas parameter is r_s. The magnetic field is B in units of B_0. The charge density is expanded in Legendre polynomials with coefficients a_l (l even). The ratios $a_2(r)/a_0(r) \times 100$ (first row) and $a_4(r)/a_0(r) \times 100$ (second row) are shown for three distances r/r_s from the test charge.

r_s	B/B_0	$r/r_s = 0.5$		$r/r_s = 1.0$		$r/r_s = 1.5$	
1	0.2	−0.0079	0.0002	−0.0080	−0.0001	0.0070	0.0033
	0.5	0.0363	−0.0001	0.0260	−0.0022	−0.0424	−0.0203
	1.0	0.0017	−0.0024	−0.1592	−0.0300	−0.2539	−0.0821
	2.0	−0.1205	−0.0078	−0.7172	−0.0742	−0.8964	−0.0968
2	0.2	−0.0028	−0.0006	0.0121	−0.0025	0.0366	−0.0006
	0.5	−0.0082	−0.0019	−0.1164	−0.0192	−0.1526	−0.0304
	1.0	0.6921	0.0272	0.8995	0.1427	0.2729	0.0854
	2.0	3.5363	0.4944	2.8790	1.9797	0.4127	1.2595
3	0.2	−0.0040	−0.0004	−0.0308	−0.0019	−0.0292	0.0029
	0.5	0.3762	0.0220	0.4400	0.1198	0.0997	0.0993
	1.0	1.6142	0.2813	0.9618	0.9077	0.0399	0.3982
	2.0	3.8058	1.5169	0.8317	1.6102	0.0252	0.3380
4	0.2	0.0656	0.0009	0.0687	−0.0003	0.0043	−0.0164
	0.5	0.6495	0.1023	0.4018	0.3561	0.0024	0.1579
	1.0	1.6397	0.6015	0.3409	0.7028	−0.0061	0.1244
	2.0	2.3485	1.8235	0.3258	0.7088	−0.0095	0.1122
5	0.2	0.1428	0.0114	0.1369	0.0570	0.0124	0.0409
	0.5	0.7130	0.2037	0.1843	0.3425	−0.0104	0.0600
	1.0	1.2175	0.7718	0.1568	0.3660	−0.0113	0.0497
	2.0	1.3141	1.4157	0.1507	0.3701	−0.0127	0.0447

4. Results

We have performed calculations for a test charge immersed in an electron gas of density corresponding to values of the electron parameter $r_s = 1$, 2, 3, 4 and 5, and for values of the magnetic field (in units of $B_0 = 2.35 \times 10^9$ G) $B/B_0 = 0.2$, 0.5, 1 and 2. The values of the chemical potential μ corresponding to these parameters are shown in the appendix, together with the description of an analytical approximation for $y = \mu/\hbar\omega$, as a function of density, which simplifies the calculation.

The results obtained for the second-order energy δE defined in (24) are shown in table 1, with and without xc effects in the response function (i.e. $X = 0$ in the second case). As a general rule, the magnitude of δE increases with the field, as displayed in figure 5. There is a discontinuity in this energy as a function of B each time a new Landau band begins to be populated, because $\chi^0(q = 0)$ is singular for the corresponding values of the field. Also, it is clear that the higher the density the weaker the relative change in energy because the rigidity of the system increases with the density. The effect of exchange and correlation on δE is important. At zero field, the xc effect goes from 3.7% at $r_s = 1$ to 9.6% at $r_s = 5$, but for the maximum field $B/B_0 = 2$, it increases from 3.9% at $r_s = 1$ to 22.5% at $r_s = 5$.

The charge density on the test charge $\delta n(0)$ is also shown in table 1. The trends are the same as for the energy. The effect of the field is small at $r_s = 1$, but considerable at $r_s = 5$, where $\delta n(0)$ changes by a factor 5.5 from $B/B_0 = 0$ to 2. The xc effect is also

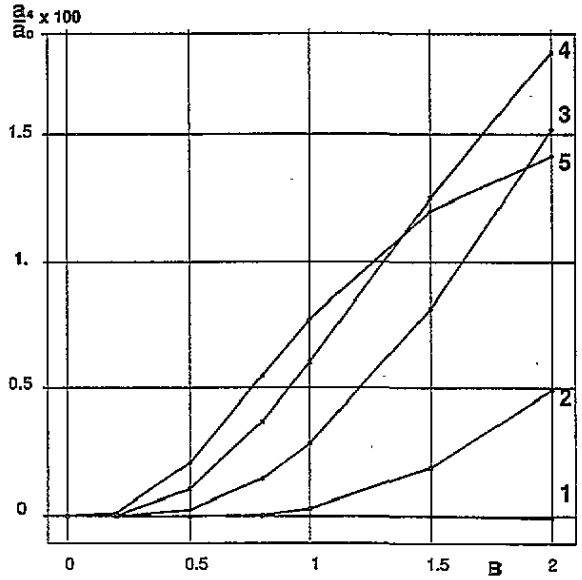

Figure 11. The same as figure 10, but for the coefficient a_4.

enhanced at low density and large field. For all the cases listed here, we have found that the careful treatment of large wave vectors in the response function is crucial in order to obtain an accurate density at the nucleus. If the numerical cut-off on q is too low, the density is underestimated and approaches the point charge with a zero slope instead of a finite slope, because the exact q^{-2} decay of the response function is replaced with an erroneous exponential decay. In figure 6 we see the charge density $\delta n(r)$ around the test charge as a function of distance r/l for $r_s = 2$ and $B/B_0 = 2$. In this case, $l = 0.707$ au. There are four curves corresponding to the angular directions $\theta = 0$ (along B), $\pi/6$, $\pi/3$ and $\pi/2$ (perpendicular to B). A last curve represents the charge density in the absence of a magnetic field. The effect of the field is very strong, as proved by the important differences between the curves with and without B. The density decreases much more slowly in the z direction, as already shown by Tomishima and Shinjo in the Thomas–Fermi theory for atoms in a strong magnetic field with inhomogeneity corrections [8]. In the present case, the non-spherical shape of the density is obvious and is a dominant character of the physical system. In figure 7, we have displayed the same curves, but for $B/B_0 = 0.2$, still at $r_s = 2$. The situation is entirely different for this low-field: the curves with and without field are almost identical. The differences $\delta n(r, B) - \delta n(r, 0)$ are magnified in figures 8 and 9.

The analysis of the non-sphericity in the charge density is shown in table 2. The ratios $a_2(r)/a_0(r) \times 100$ and $a_4(r)/a_0(r) \times 100$, at three distances r from the test charge, are given for all the r_s and B values considered in this study. These ratios increase with B, although a saturation occurs in $a_2(r)/a_0(r)$ at $B/B_0 = 1$ for $r_s = 4$ and 5, probably in favour of higher angular momenta in the expansion of (25). This effect appears clearly in figures 10 and 11, where the ratios are shown for $r/r_s = 0.5$. For magnetic fields not exceeding B_0, the non-sphericity is small at $r_s = 1$. It increases very fast with r_s. If one chooses the onset of significant non-sphericity when the ratios reach the value of 1% for $r/r_s = 0.5$, this onset occurs around $B = B_0$ (1 au) for any value of r_s.

It appears from the results reported above that, in the domain of metallic densities and

for magnetic fields larger than the reference field B_0, the non-spherical shape of the electron charge is an important physical feature. This feature should be treated accurately in any model dealing with the modifications brought by such high magnetic fields to the structure of dense electronic systems. For lower fields, a perturbation approach is sufficient.

Appendix A. An analytical approximation for the chemical potential as a function of density

The electron density n of a uniform electron gas in a magnetic field is related to the chemical potential μ by

$$n = a_0^{-3}\frac{\sqrt{2}}{\pi^2}\left(\frac{\hbar\omega}{\varepsilon_0}\right)^{3/2}\sum_{j=0}^{N}\sqrt{y-\left(j+\frac{1}{2}\right)} \tag{A1}$$

where a_0 is the Bohr radius, ω the cyclotron frequency, ε_0 the electrostatic energy e^2/a_0 and

$$y = \mu/\hbar\omega. \tag{A2}$$

N is the index of the highest occupied Landau band. Defining the reduced density

$$x = n(\pi^2/\sqrt{2})(\varepsilon_0/\hbar\omega)^{3/2} \tag{A3}$$

we have obtained expressions for $y = f_N(x)$. First, it is easy to derive *exact* expressions for the two lowest bands. In the case $N = 0$ we have

$$y = \tfrac{1}{2} + x^2$$

and in the case $N = 1$

$$y = \tfrac{3}{2} + (x^2 - 1)^2/4x^2.$$

For larger values of N, we have derived accurate *approximate* expressions. First, for a given N, one can see that, for x very large, y behaves as

$$y = [1/(N+1)^2]x^2 + O(x^0).$$

At the bottom of band N, one has obviously

$$y = y_N + (x - x_N)^2 + \text{constant}$$

with

$$y_N = N + \tfrac{1}{2} \qquad x_N = \sum_{j=0}^{N}\sqrt{j}. \tag{A4}$$

Now, when a new band opens, one must have

$$y_N + 1 = f_N(x_{N+1}).$$

The simplest expression satisfying all these constraints is

$$y = y_N + [(x^2 - x_N^2)^2/4x^2][b_N + 4a_N(x^2 - x_N^2)]/[b_N + a_N(x^2 - x_N^2)]. \tag{A5}$$

x_N and y_N are defined in (A4). The other constants are

$$a_N = 1/(N+1)^2 \tag{A6}$$

$$b_N = [4d_N/(d_N^2 - 4x_{N+1}^2)](x_{N+1}^2 - a_N d_N^2) \tag{A7a}$$

$$d_N = x_{N+1}^2 - x_N^2. \tag{A7b}$$

(A5) is general and includes also the cases $N = 0$ and 1. We have checked its numerical accuracy up to $N = 9$. An average error ε_N in each band is defined as follows. In a given band N, we use a mesh of hundred points for the variable y defined in (A2): $y_q = y_N + q/100$ ($q = 1$–100). For each of these y_q, we calculate the corresponding density x_q (A1), and then the approximate value of $y = f_N(x_q)$ (A5). The average relative error in band N is

$$\varepsilon_N = \frac{1}{y_N}\left[\frac{1}{100}\sum_{q=1}^{100}(y_q - f_N(x_q))^2\right]^{1/2}. \tag{A8}$$

The values of these errors are shown in table A1. They are of the order of 10^{-3} in the highest band considered. Thus, the numerical fit proposed is accurate enough for practical applications. It avoids the numerical solution of an implicit equation to obtain y. Once the reduced density is given, the index N of the Landau band is determined by location of x according to $x_N \leqslant x < x_{N+1}$, and then y is explicitly calculated from the approximant in (A5).

Table A1.

N	y_N	$10^3\varepsilon_N$
2	2.5	0.035
3	3.5	0.423
4	4.5	0.729
5	5.5	0.916
6	6.5	1.02
7	7.5	1.07
8	8.5	1.08
9	9.5	1.07

The values of the quantity $y - \frac{1}{2}$, related to the chemical potential, for all the cases studied in this work are listed in table A2.

Table A2.

r_s	$B/B_0 = 0.2$	$B/B_0 = 0.5$	$B/B_0 = 1$	$B/B_0 = 2$
1	8.728	3.157	1.284	0.347
2	1.901	0.347	0.434(−1)	0.542(−2)
3	0.476	0.305(−1)	0.381(−2)	0.476(−3)
4	0.847(−1)	0.542(−2)	0.678(−3)	0.847(−4)
5	0.222(−1)	0.142(−2)	0.178(−3)	0.222(−4)

References

[1] 1992 *National High Magnetic Field Laboratory Internal Report* LALP
[2] Kadomtsev B B 1970 *Sov. Phys.–JETP* **31** 945
[3] Mueller R O, Rau A R P and Spruch L 1971 *Phys. Rev. Lett.* **26** 1136
[4] Banerjee B, Constantinescu D H and Rehak P 1974 *Phys. Rev.* D **10** 2384
[5] Glossman M D and Castro E A 1988 *J. Phys. B: At. Mol. Opt. Phys.* **21** 411
[6] Tomishima Y and Yonei K 1978 *Prog. Theor. Phys.* **59** 683
[7] Yonei K and Motomochi T 1990 *J. Phys. Soc. Japan* **59** 3571

[8] Tomishima Y and Shinjo K 1979 *Prog. Theor. Phys.* **62** 853
[9] Tomishima Y, Matsuno K and Yonei K 1982 *J. Phys. B: At. Mol. Phys.* **15** 2837
[10] Lieb E H, Solovej J P and Yngvason J 1992 *Phys. Rev. Lett.* **69** 749
[11] Li S and Percus J K 1990 *Phys. Rev.* A **41** 2344
[12] Amovilli C and March N H 1991 *Phys. Rev.* A **43** 2528
[13] Vignale G and Rasolt M 1988 *Phys. Rev.* B **37** 10 685
[14] Greene M P, Lee H J, Quinn J J and Rodriguez S 1969 *Phys. Rev.* **177** 1019
[15] Glasser M L and Kaplan J I 1972 *Ann. Phys., NY* **73** 1
[16] Chiu K W and Quinn J J 1974 *Phys. Rev.* B **9** 4724
[17] Glasser M L 1983 *Phys. Rev.* B **28** 4387
[18] Skudlarski P and Vignale G 1903 *Phys. Rev.* B **48** 8547
[19] There is a considerable amount of work on the local field factor available in the literature. See for instance a brief review: Shimoji M 1977 *Liquid Metals* (London: Academic) p 105
[20] Vignale G and Skudlarski P 1992 *Phys. Rev.* B **46** 10 232